Remote Sensing of Environment xxx (2016) xxx–xxx

Contents lists available at ScienceDirect

Remote Sensing of Environment

journal homepage: www.elsevier.com/locate/rse

Landsat 8: Providing continuity and increased precision for measuring multi-decadal time series of total suspended matter

Leo Lymburner [a,*], Elizabeth Botha [b], Erin Hestir [c], Janet Anstee [b], Stephen Sagar [a], Arnold Dekker [d], Tim Malthus [e]

[a] National Earth and Marine Observation Group, Geoscience Australia, Canberra 2609, Australia
[b] CSIRO Oceans and Atmosphere Flagship, Acton, Canberra, 2601, Australia
[c] Center for Geospatial Analytics, Department of Marine, Earth and Atmospheric Sciences, North Carolina State University, Raleigh, NC, USA
[d] CSIRO Land and Water Flagship, Acton, Canberra, 2601, Australia
[e] CSIRO Oceans and Atmosphere Flagship, Dutton Park, Brisbane, 4102, Australia

ARTICLE INFO

Article history:
Received 3 July 2015
Received in revised form 28 March 2016
Accepted 10 April 2016
Available online xxxx

Keywords:
Total suspended matter
Landsat
Time series
Multi-sensor

ABSTRACT

The water clarity of many inland water bodies is under threat due to intensifying land use pressures in conjunction with changes in water levels that result from increasing demand and climate variability. The recent launch of Landsat 8 coupled with Geoscience Australia's recent reprocessing of the Landsat Thematic Mapper (TM) and Enhanced Thematic Mapper (ETM+) archives over the whole of Australia to a consistent surface reflectance product enables sub continental scale spatio-temporal analysis of freshwater optical water quality in support of monitoring and decision making for water management agencies. In this research, we present an objective assessment of the potential of Landsat 5 TM, Landsat 7 ETM+ and Landsat 8 Operational Land Imager (OLI) data for monitoring inland water quality dynamics over a number of lakes and reservoirs with a range of optical water types in New South Wales and Queensland, Australia. We used bio-optical modelling to develop sensor-specific total suspended matter (TSM) retrieval algorithms that account for the difference in relative spectral response between Landsat 7 ETM+ and Landsat 8 OLI. We were able to compare the suitability of the different sensors for optical water quality measurements using water bodies that fell within Landsat path overlaps where Landsat images of surface reflectance were acquired within 24 h between Landsat 5 TM and Landsat 7 ETM+ or Landsat 7 ETM+ and Landsat 8 OLI. These water bodies represent a range of hydrological and limnological conditions, and enabled us to assess: 1) the comparability of TSM measurements retrieved from each sensor, and 2) the surface reflectance to image noise characteristics of Landsat 7 ETM+ and Landsat 8 OLI. Comparisons of lake surface reflectance and noise equivalent reflectance difference show that the improved radiometric resolution and increased quantization of Landsat 8 OLI relative to Landsat 7 ETM+ significantly reduce image noise and spectral heterogeneity, indicating that Landsat 8 OLI data are expected to provide more precise water quality retrievals relative to Landsat 7 ETM+. We found that: 1) the TSM retrievals from the different sensors are highly comparable; 2) Landsat 5 TM overestimated TSM relative to Landsat 7 ETM+ by 6.4%; and 3) Landsat 7 ETM+ overestimated TSM relative to Landsat 8 OLI by only 1.4%. Retrieved TSM values were highly correlated with independent *in situ* data acquired within 24 h of satellite overpass ($r = 0.99$) with a mean average error of 14 mg/L. The results demonstrate that time series analysis of TSM retrievals can be conducted across a wide range of lakes at the sub-continental scale to characterise the multi-decadal TSM dynamics.

1. Introduction

Land use intensification and watershed disturbance often lead to an increase in both sediment and nutrient fluxes to rivers and other inland water bodies, and a large portion of these increased fluxes are retained in inland waters, including both lakes (Olmanson, Bauer, & Brezonik, 2008) and constructed reservoirs (Harrison, Bouwman, Mayorga, & Seitzinger, 2010; Harrison et al., 2005). Sediments and nutrients of anthropogenic origin are among the most important pollutant stressors threatening water security for human consumption and freshwater biodiversity (Davies-Colley & Smith, 2001; Foley et al., 2005; Vorosmarty et al., 2010) and affect the aesthetic value and ecological and biogeochemical function of a water body. Total suspended matter (TSM), the mass or concentration of inorganic and organic matter held in suspension, is a well recognised indicator of water quality (Bilotta & Brazier, 2008). Increased TSM in aquatic ecosystems reduce water clarity and the depth of the euphotic zone (Bilotta & Brazier, 2008; Davies-Colley

* Corresponding author.
E-mail address: leo.lymburner@ga.gov.au (L. Lymburner).

http://dx.doi.org/10.1016/j.rse.2016.04.011
0034-4257/

& Smith, 2001), impacting primary producers including phytoplankton and aquatic macrophytes, and eventually leading to an impoverished ecological status (Dennison et al., 1993; Jeppesen et al., 2009).

The Landsat series of sensors, and specifically the Landsat 5 TM, Landsat 7 ETM + and Landsat 8 OLI sensors have acquired data systematically according to a long term acquisition plan (Arvidson, Gasch, & Goward, 2001). This in combination with their 30 m spatial resolution means that the Landsat series of satellites provide a unique, freely available dataset to identify both historical baselines and current changes in TSM in relatively small water bodies across large geographic areas. Previous studies have mapped TSM using Landsat (Carpenter & Carpenter, 1983; Dekker, Vos, & Peters, 2002; Heege, Kiselev, Wettle, & Hung, 2014; Kong et al., 2015; Lulla, 1983; Mertes, Smith, & Adams, 1993). These studies, however, typically focus on a specific location, a single Landsat sensor, or a small number of scenes.

One of the greatest challenges to developing a systematic time series of TSM across large geographic regions is ensuring that the TSM estimates are not varying due to changes in sensors Barnes et al. (2014). This includes changes in spectral response functions (Fleming, 2006; Flood, 2014) as well as radiometric quality, which impacts the accuracy of the retrieval as well as the effective spatial resolution of the data (Hu et al., 2012; Hestir, Brando, Bresciani, et al., in press). Although Landsat 8 OLI has been demonstrated to have sufficient radiometric capability to measure TSM in turbid coastal waters (*e.g.*, Vanhellemont & Ruddick, 2014), the comparability of TSM retrievals across different Landsat sensors needs to be evaluated. For example, in a simulation study for turbid coastal waters, Pahlevan and Schott (2013) showed higher spatial variability and lower accuracy in TSM retrievals from Landsat 7 ETM + compared to Landsat 8 OLI due to the lower quantization of the sensor (8 bits for ETM + and 12 bits for OLI). However, they also conclude that overall the TSM products derived from the two simulated sensors were generally comparable and should be sufficient for long-term monitoring of coastal waters. Vanhellemont and Ruddick (2014) retrieved total suspended matter (TSM) from actual Landsat 8 observations of a turbid coastal environment. For Landsat 7 ETM +, however, they found it necessary to bin data to 11 × 11 pixels to overcome the limited quantization. This reduced the effective spatial resolution of Landsat 7 ETM + to 330 m, which would significantly limit the utility of Landsat for TSM time series analyses in smaller inland waterbodies.

To develop sufficiently reliable TSM time series for inland water bodies, a consistent, systematic and standardized methodology must be successfully implemented across the Landsat archive, which is comprised of multiple scenes and sensors and well characterised but variable radiometric quality (Dekker & Hestir, 2012; Malthus, Hestir, Dekker, & Brando, 2012; Markham & Helder, 2012). The development of the Australian Geoscience Data Cube (Purss et al., 2015) provides access to Landsat observations of the entire Australian continent that have all been processed using the same atmospheric correction, view angle and BRDF correction technique (Li et al., 2010) and pixel quality flagging methods (Irish, Barker, Goward, & Arvidson, 2006; Sixsmith, Oliver, & Lymburner, 2013; Zhu & Woodcock, 2012). This makes it possible to retrieve a multi-sensor time series of surface reflectance observations that have had the cloud and cloud shadows removed. The availability of this consistently processed surface reflectance dataset across Australia allows for the first time the development of a systematic, standardized methodology to estimate lake and reservoir TSM. This can now be done across large geographic areas and enables the comparison of inland water TSM retrievals across different sensors to support long-term monitoring of water bodies to identify both short term changes and long term trends in water quality.

Systematic TSM retrieval algorithm for time series of inland water bodies requires being able to apply an algorithm to Landsat data at full (30 m) resolution while accounting for the differing spectral response functions of the sensors (Flood, 2014). It also requires the automated removal of sun glint and small white cap affected observations (Devred et al., 2013; Kutser, 2012). Furthermore, retrieving TSM from many different waterbodies over a large geographic area will include lakes that span a range of optical conditions due to a variety of hydro-limnological settings. In many parts of the world, including Australia, *in situ TSM* optical water quality characterisation data are only available for a limited number of lakes. This necessitates that the systematic TSM retrieval algorithm cannot be dependent on the availability of TSM measurements necessary for an empirical approach (*e.g.* Olmanson et al., 2008) or on the inherent optical properties for each water body necessary for a full physics-based approach (*e.g.* Heege et al., 2014).

The objectives of this study are to: 1) develop a method for generating time series of TSM measurements at the multi-decadal scale using multiple Landsat sensors; 2) apply this technique to quantify the temporal dynamics of TSM of lakes distributed through a region with high variability in rainfall and climatic zones ranging from mid-latitude temperate, alpine, and semi-arid to sub-tropical; 3) evaluate the performance of the different Landsat sensors for inland water TSM retrievals across large regions to support long-term monitoring activities.

2. Method

2.1. Site description

Australia provides an excellent case study for the development of a systematic TSM retrieval approach. The continent is under high water stress due to low annual precipitation, the highest rates of surface water loss due to evapotranspiration and increasing anthropogenic water demand. It is ranked among the worst of developed countries for the way in which water resource management affects ecosystems (Emerson et al., 2012). Surface water quality in Australia is declining (Emerson et al., 2012), recurring harmful and nuisance algal blooms are widespread (Davis & Koop, 2006), nutrient fluxes and dynamics are poorly resolved (Davis & Koop, 2006), and sediment erosion and transport to freshwater ecosystems and the coastal zone remain as critical concerns (McCulloch et al., 2003; Prosser et al., 2001). Under the *Water Act 2007* and *Water Regulations 2008*, the Australia Bureau of Meteorology is responsible for reporting on Australian inland water quality. However, water quality information in Australia is sparse, difficult to obtain, and variable in content and accuracy due to the fact that it has been collected by different agencies using different sampling techniques and is constrained by different licensing conditions (Dekker & Hestir, 2012). In Australia, the states of New South Wales and Queensland have a large number of lakes and reservoirs which are measurable with Landsat pixel resolutions (Dekker & Hestir, 2012), and have some TSM measurements available. The states also span a large gradient of hydro-climatic conditions. Thus, we selected lakes and reservoirs from within the state of New South Wales and Queensland for application of systematic TSM retrieval (Fig. 1).

2.2. Water body identification

Although the spatial resolution of Landsat makes it ideal for measuring a variety of inland water bodies (Hestir, Brando, Campbell, et al., 2015), smaller water bodies are subjected to adjacency effects (Giardino, Brando, Dekker, Strömbeck, & Candiani, 2007). To ensure that only pure water reflectance was analysed in this study, only water bodies that were larger than 3 × 3 Landsat pixels were used (Table 1, Fig. 1). Subsequent to this screening, the location for the time series of surface reflectance observations for each water body was selected using the following criteria:

- Located in the deepest part of the water body (to ensure optical depth and permanent inundation in the case of water bodies with highly variable inundation regimes)
- Located as far from the shore as possible while still meeting the criterion above (to minimise the impact of adjacency effects)

Please cite this article as: Lymburner, L., et al., Landsat 8: Providing continuity and increased precision for measuring multi-decadal time series of total suspended matter, *Remote Sensing of Environment* (2016), http://dx.doi.org/10.1016/j.rse.2016.04.011

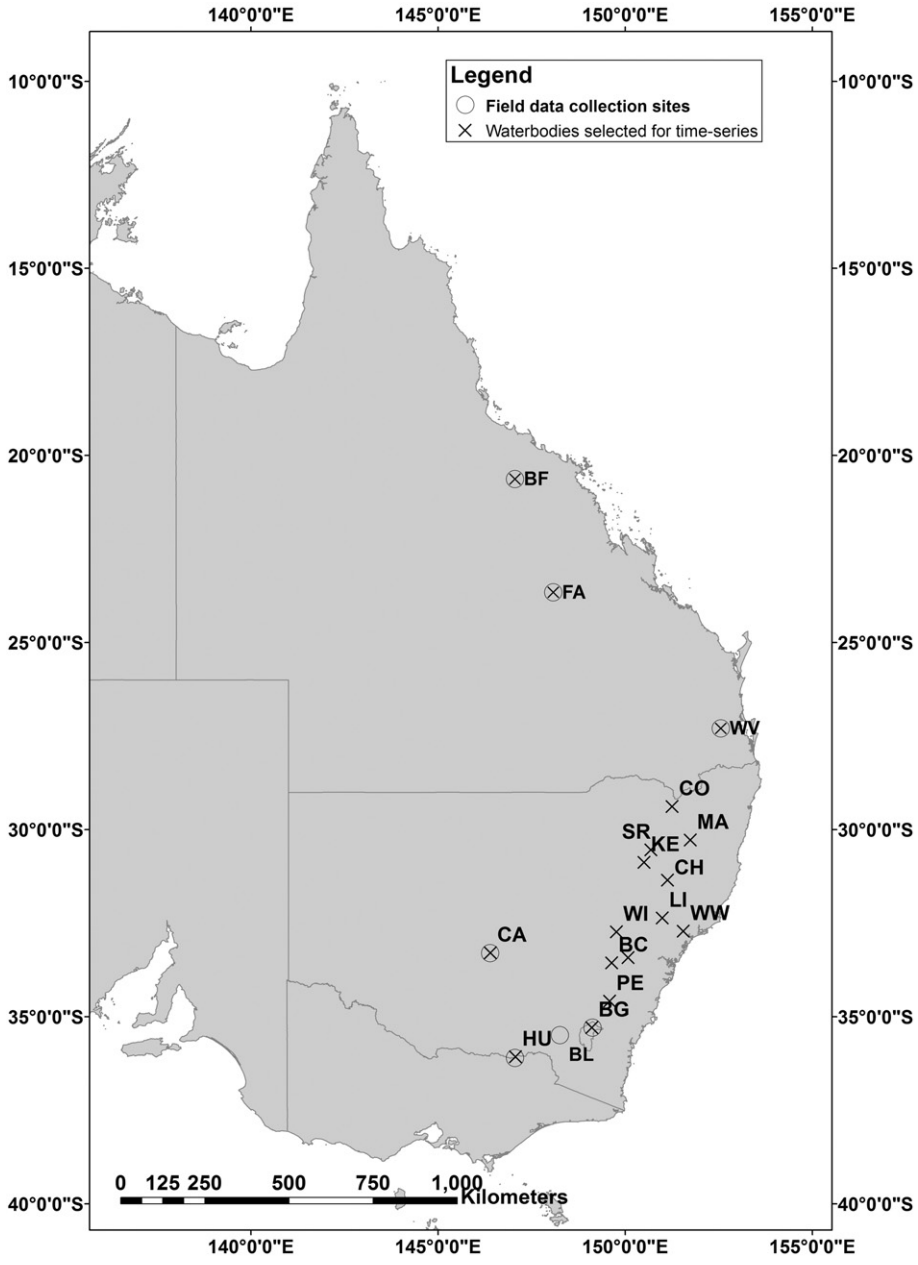

Fig. 1. Site locations for inland waters in New South Wales, Australia, waterbodies marked with X are described in Table 1. Inherent optical properties from waterbodies marked with a circle were used to establish the regional inherent optical property (IOP) set for the bio-optical modelling.

2.3. Landsat TSM retrieval

Retrieving the concentration of total suspended matter from Landsat data requires knowledge of its effects on the spectral signal measured by the sensor. Dekker et al. (2002) identified the green and red Landsat bands as most suitable for estimating variations in total suspended matter (TSM) (Eq. (1)).

$$\text{TSM index} = (\text{green} + \text{red})/2 \quad (1)$$

The paucity of concurrent *in situ* optical water quality observations precluded an empirical approach to tuning the TSM index for regional TSM retrievals. Thus we adapted the Dekker et al. (2002) TSM index following a semi-analytical approach.

Surface reflectance data were simulated in a forward radiative transfer model Ecolight 5.0 (Mobley, Sundman, Bissett, & Cahill, 2009). Simulations were based on measurements of specific inherent optical properties (SIOPs) and water quality concentrations collected during bio-optical sampling campaigns conducted by CSIRO in seven constructed reservoirs during the dry and wet season from 2012 to 2013. The reservoirs span a latitudinal gradient of nearly 16°, from temperate to tropical climate zones. The methods for sampling and sample analyses are described in Clementson, Parslow, Turnbull, McKenzie, and Rathbone (2001) and Hestir, Brando, Campbell, et al. (2015).

A four-component optical model was parameterized in Ecolight 5.0. Fifty-nine complete sets of SIOP parameters were used from the field campaign in the forward model simulations. For all simulations, the sun zenith angle was set at 30° from nadir. Wind speed was fixed at 0 m s^{-1} and the water column was assumed to be optically deep and

Please cite this article as: Lymburner, L., et al., Landsat 8: Providing continuity and increased precision for measuring multi-decadal time series of total suspended matter, *Remote Sensing of Environment* (2016), http://dx.doi.org/10.1016/j.rse.2016.04.011

Table 1
Description of the inland water bodies assessed in this study (N[a] is the number of Landsat observations acquired by any sensor over that waterbody between 1987 and 2014).

Site name	Reservoir name	Description	Storage capacity ($ML \times 10^6$)	Water-shed area (km^2)	Mean precip. (mm/yr)	N[a]	N L5 & L7 pairs	N L7 & L8 pairs
BC	Ben Chiffley	Cool temperate. Drinking water impoundment, recreation.	0.03	960	607	301	–	–
BF	Burdekin Falls	Dry tropics, portion of watershed in wet tropics. Irrigation, urban supply.	1.86	114,240	600	305	–	–
BG	Burley Griffin	Cool temperate. Urban ornamental dammed river.	0.03	184	633	466	23	9
BL	Blowering	Cool temperate/alpine. Hydro-power, irrigation and recreation.	1.63	1606	1700	451	–	–
CA	Cargelligo	Semi-arid. Diversion weir/inflow wetland.	0.004	86,554	400	543	37	11
CH	Chaffey	Warm temperate/sub-tropical. Minor dam for flood mitigation, irrigation and water supply.	0.06	420	673	301	–	–
CO	Copeton	Hot dry temperate. Hydro-power, irrigation and water supply.	1.36	5360	763	371	–	–
FA	Fairbairn	Dry tropics. Irrigation, coal washing and groundwater recharge.	1.3	16,317	600	261	–	–
HU	Hume	Warm temperate. Hydro-power, irrigation, river regulation and recreation.	3.04	15,540	700	518	–	–
KE	Keepit	Hot dry temperate. Flood mitigation, hydro-power, and irrigation.	0.43	5700	673	375	–	–
LI	Liddell	Humid sub-tropical. Artificial lake for power station cooling water.	0.15	74	654	494	46	8
MA	Malpas	Cool temperate. Water supply impoundment, recreation.	0.01	197	931	470	25	15
PE	Pejar	Cool dry temperate. Urban water supply, recreation	0.009	143	666	177	–	–
PI	Pindari	Hot temperate. Impoundment for hydro-power, flood mitigation, and irrigation.	0.31	1994	740	362	–	–
SR	Split Rock	Hot dry temperate. Impoundment for flood mitigation and irrigation.	0.4	1650	633	321	–	–
WA	Wallace	Cool temperate.	0.004	100	859	277	–	–
WI	Windamere	Warm temperate/humid subtropical. Hydro-power, irrigation and water supply.	0.37	1070	675	475	–	–
WV	Wivenhoe Dam	Humid subtropical. Flood control, hydro-power and urban supply.	2.6	7020	1000	338	–	–
WW	Walka Waterworks	Warm temperate. Former water pumping station currently used as urban recreation.	–	21,637	504.5	160	–	–

homogeneous. Inelastic scattering was excluded. The simulated reflectance spectra were then convolved to represent the spectral resolution of Landsat 5 TM, Landsat 7 ETM + and Landsat 8 OLI. This was achieved by applying the specific spectral response curves for each band for each sensor.

To ensure the accuracy of the simulated data, we compared *in situ* reflectance measurements made concurrently with the SIOP measurements with the Ecolight simulated spectra. Fig. 2 shows the measured and simulated surface water reflectance for two of the sites, CA and HU, as well as the bandwidths and positions of the Landsat sensors. For the green band Landsat 7 ETM + has a bandwidth of 0.52–0.60 μm whereas Landsat 8 OLI has a bandwidth of 0.53–0.59 μm. For the red band Landsat 7 ETM + has a bandwidth of 0.63–0.69 μm whereas Landsat 8 OLI has a narrower bandwidth of 0.64–0.67. On a per lake basis, the robustness of the optical closure between the simulated and measured spectra varied slightly by site (data not presented). Differences were likely due to the different hydro-limnological conditions of the various waterbodies where the apparent optical properties (AOPs) and IOPs were collected (Hestir, Brando, Campbell, et al., 2015) as well as variations in other environmental conditions (*e.g.*, variable atmospheric conditions, wind) that resulted in sub-optimal surface reflectance measurements.

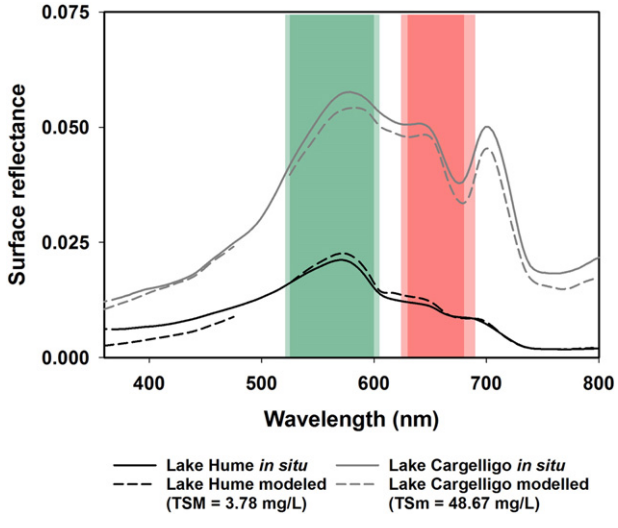

Fig. 2. Measured *in situ* water surface reflectance (solid lines) and simulated water surface reflectance (dashed lines). Two spectra are shown for Lake Hume, a dark, deep, clear reservoir, and Lake Cargelligo, a bright, shallow, turbid reservoir. The placement and bandwidth of the Landsat 5 TM, Landsat 7 ETM + and Landsat 8 OLI green and red spectral bands are indicated by the colored columns. The darker shaded column areas are sampled by all sensors and the paler areas are sampled only by Landsat 5 TM and 7 ETM +. (For interpretation of the references to color in this figure, the reader is referred to the web version of this article.)

To develop a relationship between TSM concentration and the TSM index, ten simulated spectra were selected that had the closest correlation with the concurrent *in situ* spectral measurements. The TSM concentrations associated with these spectra ranged between 1.04 and 49.67 mg/L. Fig. 3 shows the relationship between the TSM index and TSM concentrations. Similar to Dekker et al. (2002), the analytical relationship between the TSM index and TSM concentration was

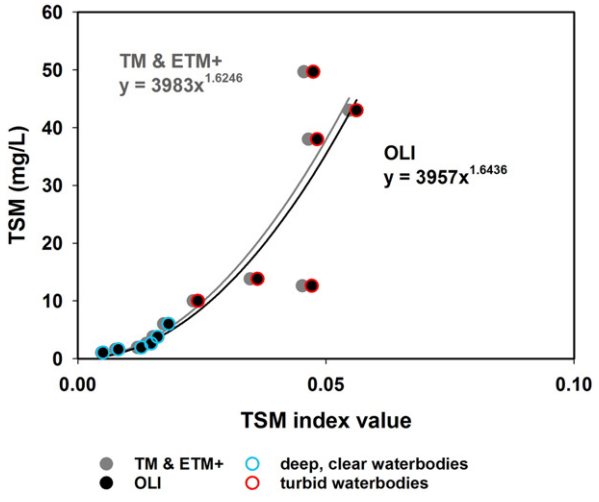

Fig. 3. The empirical relationship between TSM (mg/L) and the TSM index based on forward radiative transfer model simulations.

approximated by a power function. Thus, for processing purposes, a power function was fitted to the data to retrieve TSM concentration from Landsat surface reflectance data. In this way a semi-analytical modelling approach was used to establish an empirical relationship between *in situ* TSM and surface reflectance.

Differences in spectral response between the Landsat 5 TM and Landsat 7 ETM + sensors and the Landsat 8 OLI sensor, particularly in the width and placement of the red band implies that Landsat 8 OLI does not capture the red chlorophyll-a absorption feature centered at 676 nm in the water column in the same way as earlier Landsat sensors (Fig. 2). The result is that Landsat 8 OLI measures slightly higher red reflectance, compared to Landsats 5 TM and 7 ETM +. This difference is manifest in slightly higher TSM index values when the simulated spectra are convolved to Landsat 8 bands, compared to Landsat 7 bands (Fig. 2), particularly in more turbid waters.

2.4. Systematic image pre-processing, standardisation and observation filtering

2.4.1. Landsat pre-processing and atmospheric correction

The Landsat 5 TM, Landsat 7 ETM + and Landsat 8 OLI data used in this study were all pre-processed to a consistent geographic grid using LPGS Version 11.6.0. All images were corrected for atmospheric and BRDF effects using the method described in Li et al. (2010). The corrected images were processed to a predefined consistent grid and stored in the Australian Geoscience Data Cube (AGDC, Purss et al., 2015) which enabled the rapid retrieval of a time series of measurements from a specific location in each water body. The resultant time series provide a consistent set of surface reflectance measurements that can be compared through time.

All images were analysed to generate a corresponding 'pixel quality' image using the pixel quality flags described in (Sixsmith et al., 2013) which include cloud and cloud shadow flags generated from Automated Cloud Cover Assessment (ACCA) algorithm (Irish et al., 2006) and Fmask algorithm (Zhu & Woodcock, 2012). These pixel quality images were used to flag measurements that were contaminated by cloud/cloud shadow or band saturation. However both ACCA and Fmask sometimes fail to detect thin cloud i.e. cirrus and the edges of cumulus clouds. Surface reflectance measurements that contain undetected cloud are likely to produce erroneous results for optical water quality retrieval algorithms. A short wave infrared filtering approach was developed in this study to overcome this limitation.

2.4.2. Observation filtering using a SWIR threshold

The highly absorptive properties of water in the short wave infrared part of the spectrum are well established (Hale & Querry, 1973). The consistency of these properties means that they have been exploited to support atmospheric correction (Wang & Shi, 2005), based on the assumption that ocean pixels will provide a 'black pixel' within a MODIS scene. Wang and Shi (2005) note that the highly absorptive properties of water in the SWIR are independent of turbidity, unlike reflectance in the near infrared which increases over highly turbid water (Vanhellemont & Ruddick, 2014). Furthermore, water vapour in clouds acts to scatter the SWIR portion of sunlight, whereas liquid water absorbs it. These physical properties of water are used in this study to provide an automated quality assessment for each surface reflectance measurement. Clouds that were not detected by ACCA and Fmask were flagged by applying a very low (>1% surface reflectance) threshold to the SWIR 2 band of each sensor. This ensures that only measurements that display the very low SWIR reflectance typically associated with liquid water are included in the time series of measurements. In addition to removing undetected cloud from the time series of measurements, the SWIR threshold also screens the measurements for other artefacts that reduces the suitability of an image for water quality assessment. These artefacts include the effects of water-surface conditions, such as wind- and wave-induced sun glint and the presence of algal mats and floating macrophytes (Hestir et al., 2008; Kutser, Vahtmäe, & Praks, 2009).

2.5. Comparison of multiple Landsat sensors

During periods when two Landsat satellites are both operational and acquiring imagery the areas that fall in the overlap between adjacent paths are observed twice as often. These areas are often observed within 24 h of each other by both sensors providing a unique opportunity to compare measurements taken by different sensors over long periods of time. Four of the lakes (BG, CA, MA, LI) within the study area fell within the overlap between adjacent paths and covered a range of hydro-limnological settings (Table 1).

2.5.1. Comparing Landsat 7 & Landsat 8 noise equivalent reflectance difference

Because of the significant increase in signal to noise ratio between Landsat 7 ETM + and Landsat 8 OLI (Pahlevan et al., 2014) we assessed the difference in environmental noise equivalent reflectance difference (NEΔR) for two inland lakes. The two lakes typify the high TSM and low TSM lakes encountered in the study area thereby capturing the range of 'signal' against which to compare the NEΔR. A lower NEΔR will lead to more precise TSM retrievals which is expected to reduce uncertainty in TSM retrievals acquired by Landsat 8 OLI and upcoming high SNR sensors such as Sentinels 2 and 3 (Drusch et al., 2012). NEΔR is a measure of image noise that incorporates the signal to noise ratio of the instrument, any remaining scene-specific influences from atmospheric variability, the air-water interface and refractions of diffuse and direct sky and sunlight (Sagar et al., 2014). We selected a subset of the Landsat 7 ETM + and Landsat 8 OLI observations that had been acquired within 24 h to characterise NEΔR of the Landsat 7 ETM + and Landsat 8 OLI sensors.

NEΔR was calculated on all image pairs following a modification of the methods described in Wettle, Brando, and Dekker (2004). These methods were developed to estimate the NEΔR for images acquired over coastal waters. The method uses a pixel growing technique; sampling over a deep water region that is as homogeneous as possible to determine a band wise standard deviation. For the purposes of this investigation the application of the square kernel approach (Wettle et al., 2004) could not be applied due to the small size of inland water bodies, the presence of scan line corrector (SLC)-off gaps in the data, and heterogeneity introduced by spatial variations in the water constituents. To overcome these constraints homogenous regions in each water body were manually selected and used to calculate NEΔR. The homogenous regions were selected to exclude pixels close to the edge of lakes that might be affected by adjacency and to exclude pixels that fall within SLC-off gaps. The magnitude of the NEΔR estimates made using this homogenous region approach were then compared to those of the same sensor which could be made using the expanding kernel method, to ensure a representative NEΔR estimate had been achieved.

2.5.2. Comparison of TSM retrievals from different sensors

The TSM algorithm was applied to paired observations, acquired within 24 h of each other over both clear and turbid water bodies, to test the robustness of the methodology across all three sensors. We compared the relative performance of the different sensors for TSM retrieval by calculating the error (root mean square and mean average), bias, and non-parametric rank correlation coefficient between Landsat 5 TM and Landsat 7 ETM + as well as Landsat 7 ETM + and Landsat 8 OLI. Given the objective of the study is to develop a time series for retrospective analysis, we considered the older sensor to be the "true" value for our error and bias calculations.

Please cite this article as: Lymburner, L., et al., Landsat 8: Providing continuity and increased precision for measuring multi-decadal time series of total suspended matter, *Remote Sensing of Environment* (2016), http://dx.doi.org/10.1016/j.rse.2016.04.011

2.6. In situ validation: pseudo-matchup data

Because TSM is only a recommended water quality reporting parameter, it is not routinely monitored across water bodies in Australia (Dekker & Hestir, 2012). However, TSM were routinely monitored at Lake Burley Griffin (BG) in the Australian Capital Territory (Table 1, Fig. 1). The TSM monitoring data were collected by the National Capital Authority with support from other agencies. The monitoring program routinely monitors lake water quality during the recreational season, and makes measurements approximately monthly, usually excluding June and July. Samples are collected in an integrated tube sample from the top 5 m of the water column for range of physical, chemical, microbiological and biological analyses including measurements of TSM. The analyses of all samples were undertaken by National Association of Testing Authorities (NATA) registered laboratories. TSM observations were also collected at Blowering Reservoir (BL), Lake Hume (HU) and Fairbairn Reservoir (FA) by CSIRO and the University of South East Queensland (Table 1, Fig. 1). These samples were collected as part of field campaigns to optically characterise these waterbodies (Hestir, Brando, Bresciani, et al., in press; Hestir, Brando, Campbell, et al., 2015). Surface water was collected for a range of physical properties, including TSM. Samples were handled and analysed following the protocols described by Clementson et al. (2001).

The data were captured as part of an *in situ* water quality monitoring program, and not for the express purpose of validating EO retrievals, as a consequence the field data were acquired within 24 h of but not simultaneous with satellite overpass. As a consequence there are no concurrent matchup observations acquired at exactly the same time between Landsat overpasses and *in situ* TSM sampling. While there were no exact matchup data points between Landsat overpasses and *in situ* TSM sampling activities, we were able to identify pseudo-match up observations that were made within one day of Landsat overpass. We used the TSM data collected at sampling dates as independent *in situ* data for the TSM retrieval evaluation. We calculated the root mean square error (RMSE), mean absolute error (MAE), and percent bias for the one-day pseudo matchups.

3. Results

3.1. Noise equivalent reflectance difference

To evaluate the impact of the improved radiometric resolution on the water parameter retrievals the NEΔR values were calculated for near coincident measurements of Landsat 7 ETM+ and Landsat 8 OLI over both a deep clear water (MA) and a high suspended sediment water body (CA) (Fig. 4). Noting that although the reflectance values for each band are not continuous variables, the reflectance values for each band are connected with lines in Fig. 4 to show the shape of the spectra and to illustrate the impact that bit quantisation has on spectral shape.

The spectral heterogeneity of surface reflectance values is much greater for Landsat 7 ETM+ than for Landsat 8 OLI, and the turbid lake has greater heterogeneity than the clear lake. The NEΔR for Landsat 7 ETM+ is substantially higher than for Landsat 8 OLI, there was a nearly 25% decrease in NEΔR from Landsat 7 ETM+ to Landsat 8 OLI. The NEΔR values shown in Fig. 4 show that the improved radiometric resolution of Landsat 8 OLI has reduced the amount of noise in the Landsat 8 OLI data. The surface reflectance values also show the impact that bit quantization has on the Landsat 7 ETM+ data. The range of values observed for the areas of interest ($n = 70$ pixels) in all spectral bands is far higher for Landsat 7 ETM+ than for Landsat 8 OLI for both water bodies. These results indicate that Landsat 8 OLI data provide more

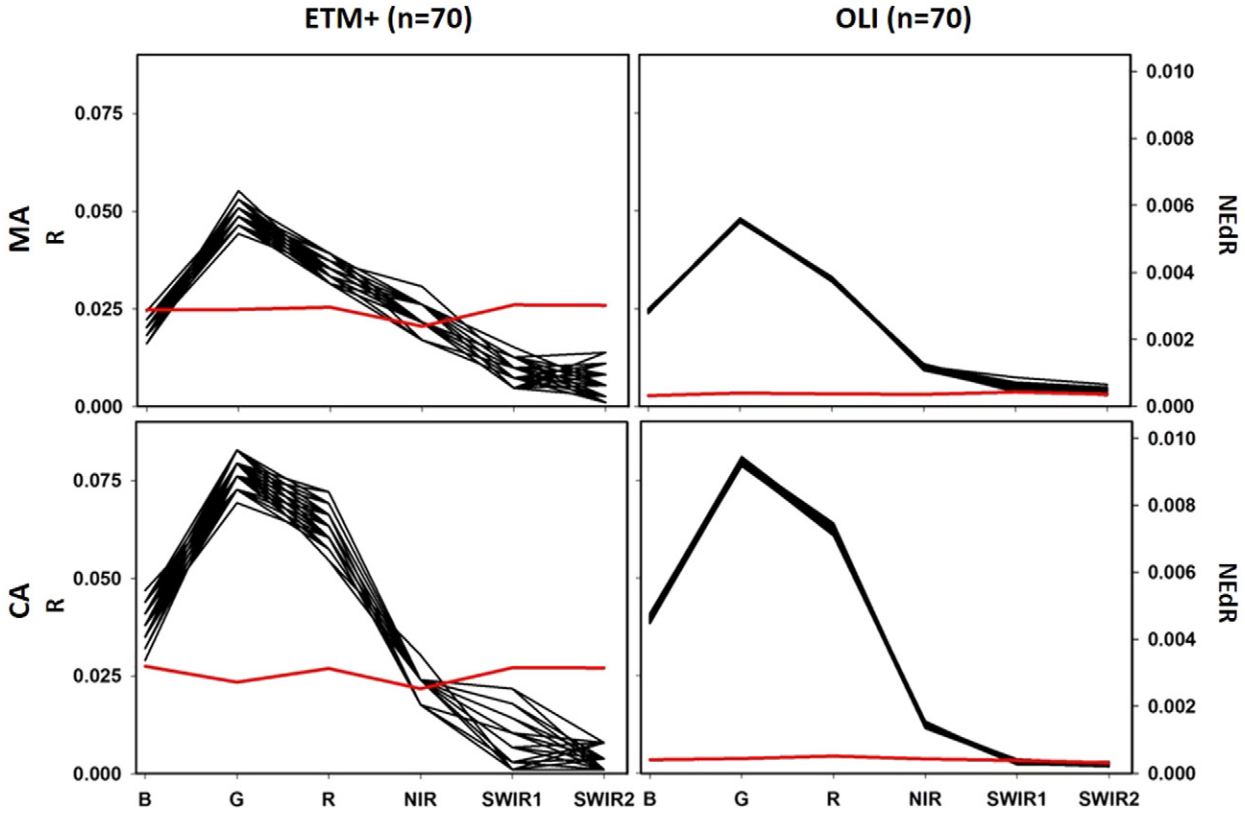

Fig. 4. Surface reflectance spectra, collected from paired Landsat 7 ETM+ and Landsat 8 OLI images, acquired within 24 h of each other over Malpas Reservoir (MA) (08 & 09/02/2014), representing a deep, clear waterbody, and Lake Cargelligo (CA) (21 & 22/07/2013), representing a water body with a high suspended sediment load. Red lines represent the NEΔR estimates, derived from a homogenous region in each water body and expressed in reflectance units on the secondary Y axis. (For interpretation of the references to color in this figure legend, the reader is referred to the web version of this article.)

Please cite this article as: Lymburner, L., et al., Landsat 8: Providing continuity and increased precision for measuring multi-decadal time series of total suspended matter, *Remote Sensing of Environment* (2016), http://dx.doi.org/10.1016/j.rse.2016.04.011

Table 2
Statistical relationship between the retrieved TSM values from paired Landsat observations acquired within 24 h.

	Number of pairs	Kendall's τ	Kendall's p-value	RMSE	MAE	Percent bias
Landsat 5 versus 7	138	0.67	<0.00	7.87	5.46	6.4
Landsat 7 versus 8	46	0.82	<0.00	7.90	4.47	1.4

consistent surface reflectance measurements which are expected to lead to more precise water parameter retrievals.

3.2. Correlation in TSM retrievals within 24 h

The correlations shown in Table 2 and in Fig. 5 show that the observations acquired by multiple sensors within the Landsat series of sensors can be used to generate comparable TSM retrievals. The relative retrieval between different sensors was not significantly different (Table 2). We found that the TSM retrievals from the different sensors are highly comparable, there was very little difference in between Landsat 5–7 and Landsat 7–8 pairs. Notably, the scatter around the 1:1 line is random rather than significantly biased in either direction. Landsat 5–7 pairs had a 6.4% bias, with Landsat 5 TM overestimating TSM relative to Landsat 7 ETM+. Landsat 7–8 pairs had only a 1.5% bias (Table 2), with Landsat 7 ETM+ overestimating TSM relative to Landsat 8 OLI. This indicates that the scatter is likely due to changes in TSM at the sample location, rather than due to a systematic difference in either of the sensor pairs.

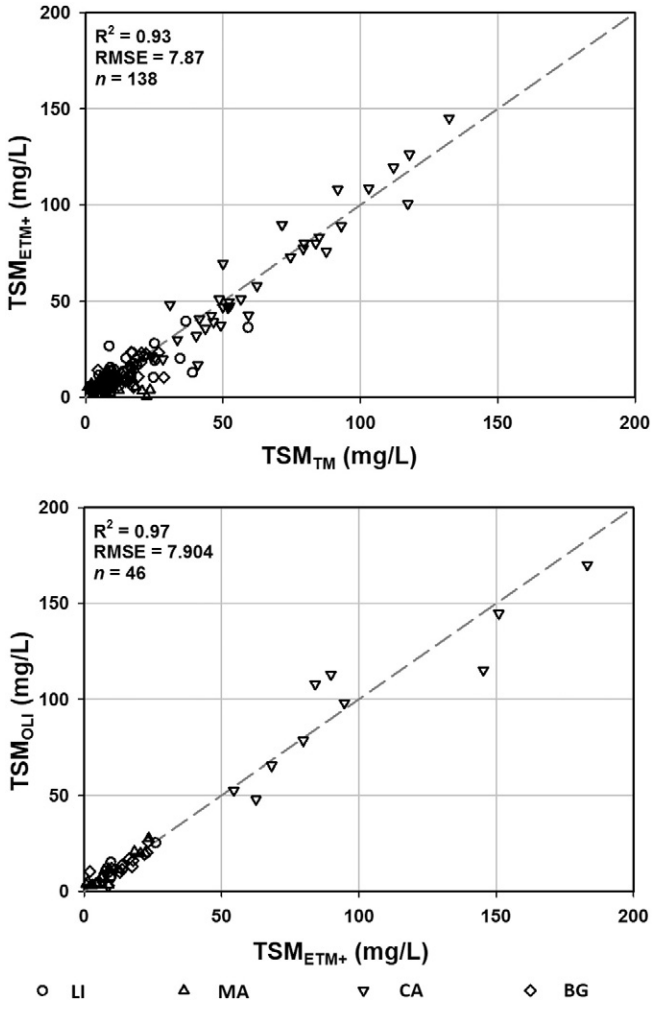

Fig. 5. The correlation between retrieved TSM values from the three Landsat sensors (Landsat 5 TM and Landsat 7 ETM+ (top) and Landsat 7 ETM+ and Landsat 8 OLI (bottom)) for observations that were acquired within 24 h of each other.

3.3. Retrieved and in situ TSM data for Lake Burley Griffin, Lake Hume, Blowering Reservoir and Fairbairn Dam

Fig. 6 shows a comparison of the *in situ* measurements of TSM for Blowering Dam (BL), Fairbairn Dam (FB), Hume Dam (HU), and Lake Burley Griffin (BG) and the TSM values retrieved from Landsat surface reflectance measurements from the field sampling locations acquired within 24 h of the *in situ* data collection. There is a strong correlation between *in situ* and satellite-retrieved TSM acquired within 24 h of one another (Pearson's correlation coefficient (r) value = 0.99) when all water bodies with available matchup data are considered). While there is a strong correlation, the retrievals for low TSM lakes such as BL show considerable scatter and there is a systematic overestimation in satellite-retrieved values (Fig. 6). A linear model fit between *in situ* and retrieved TSM yielded a slope of 0.60 ($N = 55$, standard error = 0.014, $p < 0.01$, $R^2 = 0.97$).

The systematic overestimation is most likely due to the fact that the atmospheric correction routine (Li et al., 2010) applied to the Landsat data within the Australian Geoscience Data Cube was developed for terrestrial rather than aquatic applications. An atmospheric correction routine (Vanhellemont & Ruddick, 2014) that is tailored for aquatic application was applied to a test set of images to evaluate whether this would improve retrieval accuracy. The surface reflectance values generated from the Vanhellemont and Ruddick (2014) atmospheric correction algorithm were lower than those generated by Li et al. (2010) which would reduce the overestimation bias. However in some cases the surface reflectance values generated by the Vanhellemont and Ruddick (2014) correction were negative (reflectance < 0) indicating that the code cannot be applied to a continental multi-decadal archive on an automated basis without further modification. It is beyond the scope of this paper to ensure that the Vanhellemont and Ruddick (2014) atmospheric correction routine is applicable to entire contents of the Australian Landsat archive. An atmospheric correction routine optimised for aquatic retrievals that is applicable to this archive could be developed in the future, and this would potentially lead to a reduction in the over estimation bias seen in the current results.

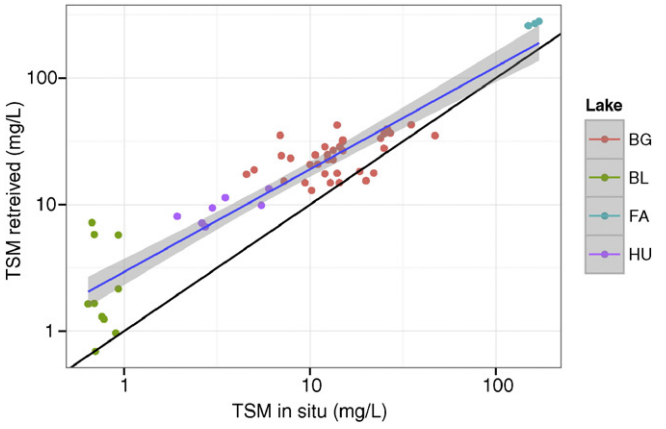

Fig. 6. A comparison of *in situ* TSM measurements and TSM values retrieved from Landsat surface reflectance.

With the exception of Lake Burley Griffin, which has had intensive long term TSM monitoring, there are not enough matchup data to evaluate the performance of the algorithm on a lake-by-lake basis. However, as is evident from Fig. 6, there is variability in how well this generalized algorithm will work across different lakes. With a mean average error of ~14 mg/L, we can assume that TSM retrievals using the generalized algorithm in highly turbid lakes or wide ranging turbidity (e.g. HU, BG, and FB) will be representative of the conditions with a likely overestimate. However, the retrievals in very clear lakes are likely to be unreliable. The lower NEΔR of Landsat 8 will likely improve the reliability of retrieval for very clear lakes however there were insufficient ($n = 1$) Landsat 8 surface reflectance measurements acquired within 24 h of *in situ* data collection to evaluate whether the lower NEΔR of Landsat 8 leads to improved retrieval precision or accuracy. This would need to be assessed in a future study once sufficient coincident or near-coincident *in situ* data has been collected.

3.4. Regional TSM dynamics

Fig. 7 shows the mean and coefficient of variation in retrieved TSM values for the period 1987 to 2014 for each lake in this study. Fig. 7 shows that reservoirs in the more elevated parts of the Great Dividing Range have predominantly lower TSM, and in some cases high c.v., whereas those lower in the landscape have higher TSM and moderate to low c.v.

The TSM time series for these two lakes are shown in Fig. 8.

Fig. 8 also shows the observation frequency differences associated with having one or two Landsat satellites acquiring data. The observation frequency during periods when two satellites are in operation is much higher, with clear observations of the Earth's surface occurring once every 10 days on average during periods of dual satellite operation compared to every 21 days during periods of single satellite operation. Please note that this 'surface' observation frequency excludes cloud affected observations and therefore differs from the 8/16 day return

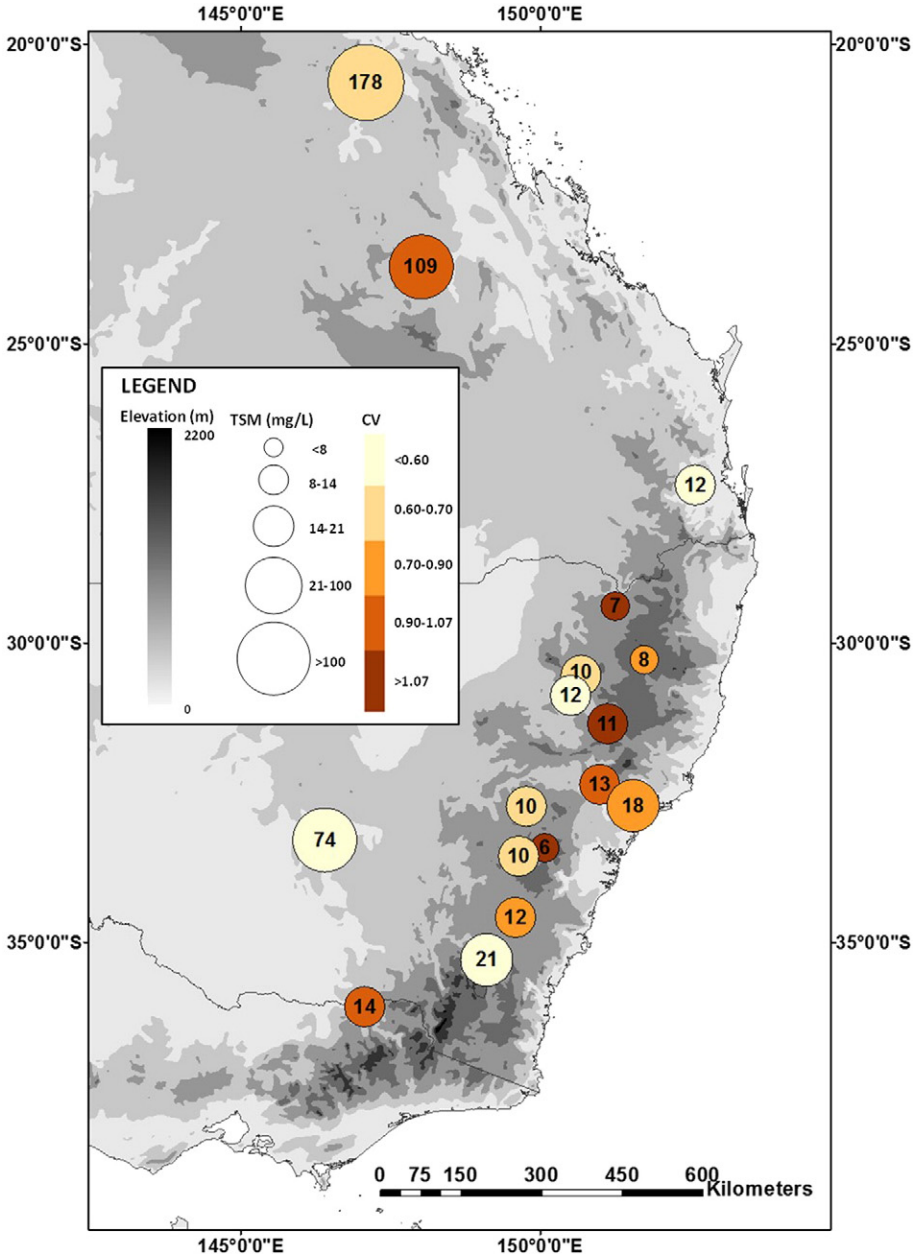

Fig. 7. The mean TSM concentration (values) and coefficient of variation (color) for the period 1987 to 2014 of the lakes within the study area. A shaded digital elevation model provides the landscape context. (For interpretation of the references to color in this figure legend, the reader is referred to the web version of this article.)

Please cite this article as: Lymburner, L., et al., Landsat 8: Providing continuity and increased precision for measuring multi-decadal time series of total suspended matter, *Remote Sensing of Environment* (2016), http://dx.doi.org/10.1016/j.rse.2016.04.011

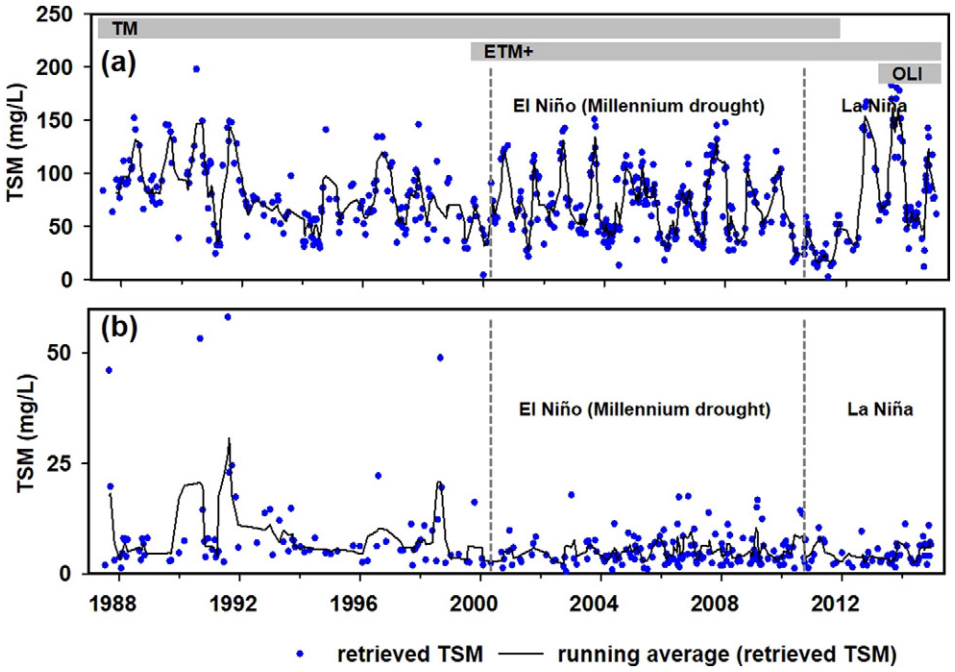

Fig. 8. A shows the TSM time series for Lake Cargelligo (CA), a lake with the high mean TSM (74 mg l^{-1}). B shows the TSM time series for Lake Wallace (WA), the lake with the lowest mean TSM (6 mg l^{-1}) in the study area. The black line represents the running mean of four values.

period of the satellite. The higher observation frequency provided by two satellites operating at the same time provides water resource managers with more timely information about lake-wide TSM dynamics.

The data in Fig. 8 are placed in the context of a climatic record (Beard, Chandler, Watkins, & Jones, 2011; Dijk et al., 2013), showing three distinct periods of TSM dynamics including periods of higher rainfall in the late 1980s through to 2000, this was followed by an extended period of low rainfall known as the Millennium drought (Dijk et al., 2013) which was in turn followed by two large flood events in 2010 and 2011 (Beard et al., 2011). Lake Cargelligo is a shallow diversion weir located in a semi-arid climate in the lower catchment, whereas Lake Wallace is an irrigation reservoir located in the upper catchment in a cool temperate climate. The lower catchment shallow lake shows persistently high (>50 mg/L) TSM with strong annual fluctuations in TSM levels with a distinct drop in 2010/11 whereas the upper catchment reservoir shows consistently low (<20 mg/L) TSM values throughout the time series with the exception of a few higher (>40 mg/L)TSM events during the 1990s.

4. Discussion

Although the radiometric resolution of earlier Landsat sensors has been limiting for retrieval of optical water quality parameters such as colored dissolved organic matter (Kutser, 2012), there was a significant change in sensor design between Landsat 7 ETM+ and Landsat 8 OLI (Morfitt et al., 2015) which is meaningful in the context of water quality applications (Pahlevan et al., 2014). The changes include a change in the relative spectral response of the sensor, and a marked increase in the radiometric resolution. The narrower red and green bands on Landsat 8 OLI alters the measurement of apparent optical properties as shown in Fig. 2 necessitating the development of sensor specific models of optically active constituents (in this case TSM) retrieval (Fig. 3). The increase in radiometric resolution is an important advance from an optical water quality retrieval point of view, given the sensitivity of some optical water quality retrieval techniques to system-wide noise (Wettle et al., 2004), and Fig. 4 shows how the improved radiometric resolution markedly improves the signal to noise equivalent reflectance difference (NEΔR) ratio. The improved signal to noise characteristics of Landsat 8 will lead to more precise TSM retrievals, but there is currently insufficient *in situ* data-to-imagery match ups to evaluate the accuracy of the Landsat 8 retrievals.

Fig. 5 shows that, once differences in relative spectral response have been taken into account, retrieved TSM values that have been observed within 24 h of each other show a high degree of correlation between sensor pairs (Landsat 5 TM and Landsat 7 ETM+, Landsat 7 ETM+ and Landsat 8 OLI). This indicates that Landsat 8 will continue to add and build on the multi-decadal record of Landsat observations of inland water quality. Furthermore, the NEΔR analysis on paired Landsat observations show the improvement in signal to noise characteristics of the Landsat 8 OLI sensor. This is consistent with recent studies for long term monitoring in coastal waters (Pahlevan et al., 2014; Vanhellemont & Ruddick, 2014).

The results from our study show that it is possible to construct a multi-sensor time series of TSM retrievals that can be used to track the relative changes in TSM within a water body with consistent errors across time and across sensors. The TSM time series do provide valuable insight into the multi-decadal dynamics of TSM concentration over time within waterbodies (Fig. 8).

The bio-optical modelling approach provided a basis for constructing a multi-sensor regionally-parameterized TSM retrieval algorithm that can be applied to a region that has scarce *in situ* measurements that would be required for the parameterization of a either a semi-empirical or fully physics based retrieval (Malthus et al., 2012). The lack of *in situ* data is not a challenge unique to Australia. Many parts of the world, in particular remote areas and developing countries, lack the basic infrastructure and resources to consistently monitor inland water quality. Regional parameterizations of retrievals based on bio-optical modelling provide a physically based approach that can be applied for first-order TSM measurement and monitoring purposes.

A comparison of the independent *in situ* data and retrieved TSM values acquired within 24 h of each other (Fig. 6) shows a strong correlation ($R^2 = 0.97$). This is an improvement on the results reported in Olmanson et al. (2008) which reported an R^2 of 0.78 correlation between surface reflectance and another measure of water clarity (Secchi disk depth) for their calibration data. However Fig. 6 also shows that the retrievals are overestimating the TSM concentrations, and are unreliable

Please cite this article as: Lymburner, L., et al., Landsat 8: Providing continuity and increased precision for measuring multi-decadal time series of total suspended matter, *Remote Sensing of Environment* (2016), http://dx.doi.org/10.1016/j.rse.2016.04.011

at very low TSM concentrations. Based on this, caution should be applied when comparing the absolute value of TSM retrievals between waterbodies. Users may choose to apply an empirical correction coefficient to account for the over estimation bias. The retrieved TSM values for very clear waterbodies are likely to be noisy, particularly for values retrieved from Landsat 5 TM and Landsat 7 ETM+ data. Retrievals from Landsat 8 OLI are less noisy due to the lower NEΔR. The accuracy of retrievals may also be improved in the future through the use of water body specific IOPs where available.

The approach presented in this paper would provide input into an analytical framework that places observed TSM dynamics into the context of the various drivers that determine water body TSM dynamics including:

- intra-year variations in stream flows/sediment flux (seasonal rainfall/stream flow patterns)
- inter-year variations in stream flows/sediment flux (climate variability, changing patterns of rainfall timing/intensity, cycles of drought and flood)
- landscape setting (upland vs lowland)
- changes in land use/catchment management
- land use intensification
- improvements in catchment management including reduced grazing pressure and water sensitive urban design.

Such a system would provide a basis for interpreting and distinguishing between the different causal factors that create the changes in TSM observed across New South Wales and Queensland (Fig. 7).

The approach developed in this paper could be applied to low to mid latitude areas. However, caution should be used in applying this approach at higher latitudes where lower solar angles reduce the signal levels, especially for Landsat 5 TM and Landsat 7 ETM+ data. The variable depth of the global Landsat archive (Kovalskyy & Roy, 2013) will determine the maximum possible length of the baseline characterisation of TSM for each lake. However the on-board storage, downlink and central storage capabilities of Landsat 8 OLI and associated ground segment enables the global availability of high SNR data (Roy et al., 2014) which will enable the capacity to characterise the TSM dynamics of water bodies worldwide.

5. Conclusions

This paper demonstrates that Landsat 8 OLI provides continuity of surface reflectance measurement enabling the long term characterisation of TSM dynamics for lakes that represent a wide range of hydrolimnological conditions. The changes in Landsat 8 OLI sensor design necessitate the development of sensor specific TSM retrieval algorithms to account for the differences in relative spectral response between Landsat 7 ETM+ and Landsat 8 OLI. However the improved SNR of Landsat 8 OLI improves the precision of TSM retrievals. Lakes that sit in the overlap between adjacent passes were observed by two Landsat sensors within 24 h during periods when two sensors are operating. The retrieved TSM values for these paired observations show that retrieved values are consistent across sensors, providing the basis for multi-sensor time series of TSM observations. Multi-sensor time series were calculated for a number of lakes in New South Wales and Queensland, Australia, using an empirical relationship developed using semi-analytical techniques developed using IOPs from lakes across the study area. The multi-decadal dynamics of TSM was captured for these lakes based on the mean and coefficient of variation in TSM for each lake. The TSM time series for high and low mean TSM values showed annual to decadal scale variability in TSM levels. The retrieved TSM values correlate strongly with the *in situ* TSM measurements acquired within 24 h of satellite overpass (Pearson's correlation coefficient (r) value = 0.99), but the retrieved TSM values were over-estimating TSM in comparison with *in situ* data. The offset between the *in situ* and retrieved TSM values indicates that an atmospheric correction routine designed for aquatic applications that can be applied at continental scales on an automated basis needs to be developed and that specific water body IOPs may be needed to increase the accuracy of retrievals in some instances. Furthermore the capacity to develop sensor specific retrieval models is crucial in the context of upcoming Sentinel 2 and Sentinel 3 missions that will augment the capacity of the Landsat series of sensors to characterise global lake water quality dynamics into the future.

Acknowledgements

The authors wish to thank the three reviewers for their comments and recommendations which have strengthened the paper.

The National Capital Authority (NCA), CSIRO and University of Southern Queensland are thanked for the provision of *in situ* measurements from their water quality sampling program from 1966 to the current time.

This research was undertaken with the assistance of resources from the National Computational Infrastructure (NCI), which is supported by the Australian Government.

This paper published with permission of the CEO, Geoscience Australia.

References

Arvidson, T., Gasch, J., & Goward, S. N. (2001). Landsat 7's long-term acquisition plan—An innovative approach to building a global imagery archive. *Remote Sensing of Environment*, *78*, 13–26.

Barnes, B. B., Hu, C., Holekamp, K. L., Blonski, S., Spiering, B. A., Palandro, D., & Lapointe, B. (2014). Use of Landsat data to track historical water quality changes in Florida Keys marine environments. *Remote Sensing of Environment*, *140*, 485–496.

Beard, G., Chandler, E., Watkins, A. B., & Jones, D. A. (2011). How does the 2010–11 La Niña compare with past La Niña events? *Bulletin of the Australian Meteorological and Oceanographic Society*, *24*, 17–20.

Bilotta, G. S., & Brazier, R. E. (2008). Understanding the influence of suspended solids on water quality and aquatic biota. *Water Research*, *42*, 2849–2861.

Carpenter, D. J., & Carpenter, S. M. (1983). Modeling inland water quality using Landsat data. *Remote Sensing of Environment*, *13*, 345–352.

Clementson, L. A., Parslow, J. S., Turnbull, A. R., McKenzie, D. C., & Rathbone, C. E. (2001). Optical properties of waters in the Australasian sector of the Southern Ocean. *Journal of Geophysical Research, Oceans*, *106*, 31611–31625.

Davies-Colley, R. J., & Smith, D. G. (2001). Turbidity suspended sediment, and water clarity: A review. *JAWRA Journal of the American Water Resources Association*, *37*, 1085–1101.

Davis, J., & Koop, K. (2006). Eutrophication in Australian rivers, reservoirs and estuaries — A southern hemisphere perspective on the science and its implications. *Hydrobiologia*, *559*, 23–76.

Dekker, A. G., & Hestir, E. L. (2012). *Evaluating the feasibility of systematic inland Water quality monitoring with satellite remote sensing.* In Canberra, Australia: Commonwealth Scientific and Industrial Research Organization, 123.

Dekker, A. G., Vos, R. J., & Peters, S. W. M. (2002). Analytical algorithms for lake water TSM estimation for retrospective analyses of TM and SPOT sensor data. *International Journal of Remote Sensing*, *23*, 15–35.

Dennison, W. C., Orth, R. J., Moore, K. A., Stevenson, J. C., Carter, V., Kollar, S., ... Batiuk, R. A. (1993). Assessing Water quality with submersed aquatic vegetation. *Bioscience*, *43*, 86–94.

Devred, E., Turpie, K., Moses, W., Klemas, V., Moisan, T., Babin, M., ... Jo, Y. -H. (2013). Future retrievals of water column bio-optical properties using the Hyperspectral Infrared Imager (HyspIRI). *Remote Sensing*, *5*, 6812–6837.

Dijk, A. I., Beck, H. E., Crosbie, R. S., Jeu, R. A., Liu, Y. Y., Podger, G. M., ... Viney, N. R. (2013). The Millennium Drought in southeast Australia (2001–2009): Natural and human causes and implications for water resources, ecosystems, economy, and society. *Water Resources Research*, *49*, 1040–1057.

Drusch, M., Del Bello, U., Carlier, S., Colin, O., Fernandez, V., Gascon, F., ... Bargellini, P. (2012). Sentinel-2: ESA's optical high-resolution mission for GMES operational services. *Remote Sensing of Environment*, *120*, 25–36.

Emerson, J., Hsu, A., Levy, M., de Sherbinin, A., Mara, V., Esty, D., & Jiteh, M. (2012). *Environmental performance index and pilot trend environmental performance index.* New Haven: Yale Center for Environmental Law and Policy.

Fleming, D. J. (2006). Effect of relative spectral response on multi-spectral measurements and NDVI from different remote sensing systems. *Geography*. College Park, MD: University of Maryland.

Flood, N. (2014). Continuity of reflectance data between Landsat-7 ETM+ and Landsat-8 OLI, for both top-of-atmosphere and surface reflectance: A study in the Australian landscape. *Remote Sensing*, *6*, 7952–7970.

Foley, J. A., DeFries, R., Asner, G. P., Barford, C., Bonan, G., Carpenter, S. R., ... Snyder, P. K. (2005). Global consequences of land use. *Science*, *309*, 570–574.

Giardino, C., Brando, V. E., Dekker, A. G., Strömbeck, N., & Candiani, G. (2007). Assessment of water quality in Lake Garda (Italy) using Hyperion. *Remote Sensing of Environment*, *109*, 183–195.

Hale, G. M., & Querry, M. R. (1973). Optical constants of Water in the 200 nm to 2000 nm wavelength region. *Applied Optics*, *12*, 555–563.

Harrison, J. A., Bouwman, A. F., Mayorga, E., & Seitzinger, S. (2010). Magnitudes and sources of dissolved inorganic phosphorus inputs to surface fresh waters and the coastal zone: A new global model. *Global Biogeochemical Cycles*, *24*, 1.

Harrison, J. A., Seitzinger, S. P., Bouwman, A. F., Caraco, N. F., Beusen, A. H. W., & Vörösmarty, C. J. (2005). Dissolved inorganic phosphorus export to the coastal zone: Results from a spatially explicit, global model. *Global Biogeochemical Cycles*, *19*, 4.

Heege, T., Kiselev, V., Wettle, M., & Hung, N. N. (2014). Operational multi-sensor monitoring of turbidity for the entire Mekong Delta. *International Journal of Remote Sensing*, *35*, 2910–2926.

Hestir, E. L., Brando, V., Bresciani, M., Giardino, C., Matta, E., Villa, P., & Dekker, A. (2015). Measuring freswater aquatic ecosystems: The need for a hyperspectral global mapping satellite mission. *Remote Sensing of Environment* in press.

Hestir, E. L., Brando, V., Campbell, G., Dekker, A., & Malthus, T. (2015). The relationship between dissolved organic matter absorption and dissolved organic carbon in reservoirs along a temperate to tropical gradient. *Remote Sensing of Environment*, *156*, 395–402.

Hestir, E. L., Khanna, S., Andrew, M. E., Santos, M. J., Viers, J. H., Greenberg, J. A., ... Ustin, S. L. (2008). Identification of invasive vegetation using hyperspectral remote sensing in the California Delta ecosystem. *Remote Sensing of Environment*, *112*, 4034–4047.

Hu, C., Feng, L., Lee, Z., Davis, C. O., Mannino, A., McClain, C. R., & Franz, B. A. (2012). Dynamic range and sensitivity requirements of satellite ocean color sensors: Learning from the past. *Applied Optics*, *51*, 6045–6062.

Irish, R. R., Barker, J. L., Goward, S. N., & Arvidson, T. (2006). Characterization of the Landsat-7 ETM+ automated cloud-cover assessment (ACCA) algorithm. *Photogrammetric Engineering and Remote Sensing*, *72*, 1179–1188.

Jeppesen, E., Kronvang, B., Meerhoff, M., Søndergaard, M., Hansen, K. M., Andersen, H. E., ... Olesen, J. E. (2009). Climate change effects on runoff, catchment phosphorus loading and lake ecological state, and potential adaptations. *Journal of Environmental Quality*, *38*, 1930–1941.

Kong, J., Sun, X., Wang, W., Du, D., Chen, Y., & Yang, J. (2015). An optimal model for estimating suspended sediment concentration from Landsat TM images in the Caofeidian coastal waters. *International Journal of Remote Sensing*, 1–16.

Kovalskyy, V., & Roy, D. P. (2013). The global availability of Landsat 5 TM and Landsat 7 ETM+ land surface observations and implications for global 30 m Landsat data product generation. *Remote Sensing of Environment*, *130*, 280–293.

Kutser, T. (2012). The possibility of using the Landsat image archive for monitoring long time trends in coloured dissolved organic matter concentration in lake waters. *Remote Sensing of Environment*, *123*, 334–338.

Kutser, T., Vahtmäe, E., & Praks, J. (2009). A sun glint correction method for hyperspectral imagery containing areas with non-negligible water leaving NIR signal. *Remote Sensing of Environment*, *113*, 2267–2274.

Li, F., Jupp, D. L., Reddy, S., Lymburner, L., Mueller, N., Tan, P., & Islam, A. (2010). An evaluation of the use of atmospheric and BRDF correction to standardize Landsat data. *IEEE Journal of Selected Topics in Applied Earth Observations and Remote Sensing*, *3*, 257–270.

Lulla, K. (1983). The Landsat satellites and selected aspects of physical geography. *Progress in Physical Geography*, *7*, 1–45.

Malthus, T. J., Hestir, E. L., Dekker, A. G., & Brando, V. E. (2012). The case for a global inland water quality product. *Geoscience and Remote Sensing Symposium (IGARSS), 2012 IEEE International* (pp. 5234–5237).

Markham, B. L., & Helder, D. L. (2012). Forty-year calibrated record of earth-reflected radiance from Landsat: A review. *Remote Sensing of Environment*, *122*, 30–40.

McCulloch, M., Fallon, S., Wyndham, T., Hendy, E., Lough, J., & Barnes, D. (2003). Coral record of increased sediment flux to the inner Great Barrier Reef since European settlement. *Nature*, *421*, 727–730.

Mertes, L. A. K., Smith, M. O., & Adams, J. B. (1993). Estimating suspended sediment concentrations in surface waters of the Amazon River wetlands from Landsat images. *Remote Sensing of Environment*, *43*, 281–301.

Mobley, C. D., Sundman, L. K., Bissett, W. P., & Cahill, B. (2009). Fast and accurate irradiance calculations for ecosystem models. *Biogeosciences Discussions*, *6*, 10625–10662.

Morfitt, R., Barsi, J., Levy, R., Markham, B., Micijevic, E., Ong, L., ... Vanderwerff, K. (2015). Landsat-8 Operational Land Imager (OLI) radiometric performance on-orbit. *Remote Sensing*, *7*, 2208–2237.

Olmanson, L. G., Bauer, M. E., & Brezonik, P. L. (2008). A 20-year Landsat water clarity census of Minnesota's 10,000 lakes. *Remote Sensing of Environment*, *112*, 4086–4097.

Pahlevan, N., Lee, Z., Wei, J., Schaaf, C. B., Schott, J. R., & Berk, A. (2014). On-orbit radiometric characterization of OLI (Landsat-8) for applications in aquatic remote sensing. *Remote Sensing of Environment*, *154*, 272–284.

Pahlevan, N., & Schott, J. R. (2013). Leveraging EO-1 to evaluate capability of new generation of Landsat sensors for coastal/inland water studies. *IEEE Journal of Selected Topics in Applied Earth Observations and Remote Sensing*, *6*, 360–374.

Prosser, I. P., Rutherfurd, I. D., Olley, J. M., Young, W. J., Wallbrink, P. J., & Moran, C. J. (2001). Large-scale patterns of erosion and sediment transport in river networks, with examples from Australia. *Marine and Freshwater Research*, *52*, 81–99.

Purss, M. B., Lewis, A., Oliver, S., Ip, A., Sixsmith, J., Evans, B., ... Chan, T. (2015). Unlocking the Australian Landsat Archive–from dark data to high performance data infrastructures. *Geographical Research Journal*, *6*, 135–140.

Roy, D. P., Wulder, M. A., Loveland, T. R., C.E., W., Allen, R. G., Anderson, M. C., ... Zhu, Z. (2014). Landsat-8: Science and product vision for terrestrial global change research. *Remote Sensing of Environment*, *145*, 154–172.

Sagar, S., Brando, V., & Sambridge, M. (2014). Noise Estimation of Remote Sensing Reflectance Using a Segmentation Approach Suitable for Optically Shallow Waters. *IEEE Transactions on Geoscience and Remote Sensing*, *52*, 7504–7512.

Sixsmith, J., Oliver, S., & Lymburner, L. (2013). A hybrid approach to automated Landsat pixel quality. *Geoscience and Remote Sensing Symposium (IGARSS), 2013 IEEE International* (pp. 4146–4149). Melbourne: VIC IEEE.

Vanhellemont, Q., & Ruddick, K. (2014). Turbid wakes associated with offshore wind turbines observed with Landsat 8. *Remote Sensing of Environment*, *145*, 105–115.

Vorosmarty, C. J., McIntyre, P. B., Gessner, M. O., Dudgeon, D., Prusevich, A., Green, P., ... Davies, P. M. (2010). Global threats to human water security and river biodiversity. *Nature*, *467*, 555–561.

Wang, M., & Shi, W. (2005). Estimation of ocean contribution at the MODIS near-infrared wavelengths along the east coast of the U.S.: Two case studies. *Geophysical Research Letters*, *32*, L13606.

Wettle, M., Brando, V. E., & Dekker, A. G. (2004). A methodology for retrieval of environmental noise equivalent spectra applied to four Hyperion scenes of the same tropical coral reef. *Remote Sensing of Environment*, *93*, 188–197.

Zhu, Z., & Woodcock, C. E. (2012). Object-based cloud and cloud shadow detection in Landsat imagery. *Remote Sensing of Environment*, *118*, 83–94.

Please cite this article as: Lymburner, L., et al., Landsat 8: Providing continuity and increased precision for measuring multi-decadal time series of total suspended matter, *Remote Sensing of Environment* (2016), http://dx.doi.org/10.1016/j.rse.2016.04.011